Astragaloside IV inhibits nasopharyngeal carcinoma progression by inhibiting SATB2/Wnt/PD-L1 pathway and enhancing the killing activity of T cells

Yinping Zeng,* Jiajun Huang,* Tingting Duan, Xiaofeng Wang

Department of Otorhinolaryngology Head and Neck Surgery, The First Affiliated Hospital of Hainan Medical University, Haikou, Hainan Province, China

*These authors share first authorship

ABSTRACT

Astragaloside IV (AS IV) inhibits the malignant phenotype of nasopharyngeal carcinoma (NPC), but whether its mechanism involves the regulation of immune checkpoint programmed cell death-ligand 1 (PD-L1) is not clear. Human NPC cells were treated with AS IV. The effects of AS IV on PD-L1 expression were assessed using RT-qPCR and Western blot. SATB2/Wnt/β-catenin signaling axis regulation was analyzed by siRNA interference, plasmid overexpression and Wnt pathway inhibitor DKK-1. T cell killing activity and tumor malignant phenotype were evaluated by LDH release, ELISA, flow cytometry and Transwell experiments. huHSC-NCG tumor-bearing mice were established to detect tumor growth, immune cell infiltration and related protein expression. AS IV dose-dependently inhibited PD-L1 expressions within NPC cells, and enhanced the activation and killing function of $CD8^+$ T cells. Mechanism studies have shown that AS IV significantly lowered the expression of SATB2, thereby inhibiting Wnt/β-catenin axis and c-MYC and Axin2 expressions, and ultimately reducing PD-L1 levels. Overexpression of SATB2 reversed AS IV's suppression of this signaling and PD-L1. Animal experiments confirmed that AS IV effectively inhibited tumor growth, enhanced $CD8^+$ T cell infiltration and activity within tumor tissues, and down-regulated the SATB2/β-catenin/PD-L1 signal axis. AS IV inhibited PD-L1 expression in NPC via targeting the SATB2/Wnt/β-catenin axis, thereby activating $CD8^+$ T cells, amplifying immunological responses, and ultimately inhibiting NPC growth.

Key words: Astragaloside IV; nasopharyngeal carcinoma; PD-L1; SATB2/Wnt/β-catenin pathway; $CD8^+$ T cells.

Correspondence: Xiaofeng Wang, Department of Otorhinolaryngology Head and Neck Surgery, The First Affiliated Hospital of Hainan Medical University, Haikou 570102, Hainan Province, China. E- mail: Wxf8141@163.com

Contributions: Yinping Zeng developed and planned the study, performed experiments, and interpreted results, edited and refined the manuscript with a focus on critical intellectual contributions. Jiajun Huang, Tingting Duan participated in collecting, assessing, and interpreting the date, made significant contributions to date interpretation and manuscript preparation. Xiaofeng Wang provided substantial intellectual input during the drafting and revision of the manuscript.

Conflicts of interest: the authors declare no conflicts of interest and all authors confirm accuracy.

Ethics approval: this study was approved by The First Affiliated Hospital of Hainan Medical University Ethics Committee (No. 2024-KYL-123).

Data Availability: the data supporting the findings of this study can be obtained from the corresponding author, upon request.

Funding: the 2024 Hainan Provincial Natural Science Foundation Project "Effect of SMG-1 on radiosensitivity of head and neck squamous cell carcinoma and its signaling pathway" (No. 820MS141).

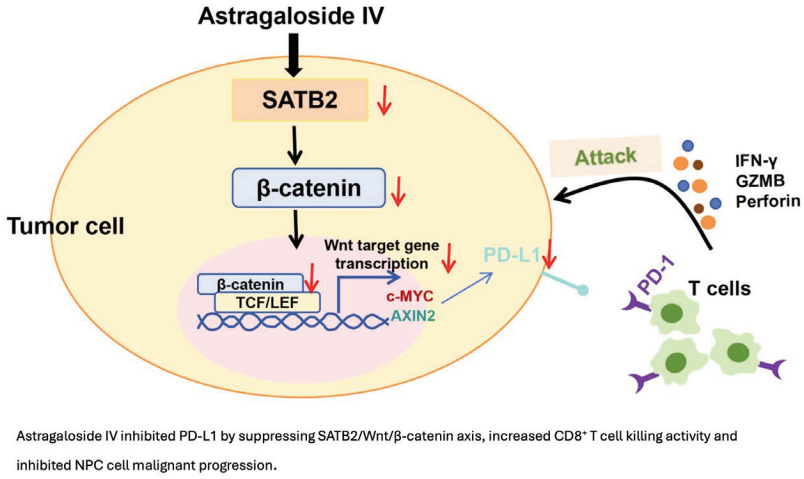

Astragaloside IV inhibited PD-L1 by suppressing SATB2/Wnt/β-catenin axis, increased CD8⁺ T cell killing activity and inhibited NPC cell malignant progression.

Graphical abstract.

Introduction

Nasopharyngeal carcinoma (NPC) is a malignant tumor originating from the nasopharyngeal epithelium. It has obvious regional and ethnic differences, with high morbidity and mortality, and frequently occurs in people over 50 years old.[1-3] NPC is a common malignant tumor in Southeast Asia and South China.[4] NPC has no obvious symptoms in the early stage, and many patients are diagnosed at an advanced stage. The survival rate for patients with advanced nasopharyngeal carcinoma is lower than that of early stage, with a 5-year overall survival rate of only 26%.[5] Currently, NPC primary treatments are chemotherapy and surgical treatment, and the prognosis of patients remains poor.[3] Different from traditional treatment methods, immunotherapy is committed to activating the patient's immune system and relying on its own immune function to fight cancer cells.[6] Programmed cell death protein 1 (PD-1) / programmed cell death-ligand 1 (PD-L1) inhibitors have been a research hotspot in tumor immunotherapy in recent years.[7] PD-L1 acts as an immunosuppressive factor. By binding to PD-1, T cells recognize cancer cells as normal cells, thereby achieving immune escape.[8] In NPC, high PD-L1 expressions are strongly associated with unfavorable prognosis and the formation of immunosuppressive microenvironments, making it an important therapeutic target.[9,10] Previous studies have shown that inhibiting PD-L1 in NPC can significantly enhance the cytotoxic T cell ($CD8^+$ T cells) killing effect on cancer cells.[11] Therefore, investigating the mechanisms of regulating the $CD8^+$ T cell killing effect on tumors is expected to provide novel targets for tumor immunotherapy.

Wnt/β-catenin signal is the classical axis that regulates cell proliferation, differentiation and stem cell self-renewal. Its abnormal activation is closely related to tumorigenesis, invasion and immune escape.[12,13] Studies have confirmed that this pathway is abnormally activated in NPC, which has a significant impact on NPC development.[14,15] This signaling promotes PD-L1 expression in cancer cells through a variety of mechanisms.[16,17] Importantly, the transcription factor Special AT-rich sequence-binding protein 2 (SATB2), as a critical factor in chromatin remodeling and gene expression regulation, is abnormally overexpressed in various malignant tumors.[18,19] It has been reported that SATB2 can regulate this pathway and promote cancer progression.[20,21] It is particularly noteworthy that SATB2 is also highly expressed in NPC, and SATB2 overexpression can significantly increase Wnt signaling pathway-related proteins.[22] Therefore, the SATB2/Wnt/β-catenin axis may be strongly associated with the malignant phenotype of NPC cells.

Astragaloside IV (AS IV) is the primary active component of Astragalus membranaceus, exhibiting anti-inflammatory, immune regulation and anti-tumor activities.[23,24] AS IV can inhibit tumor cell growth, invasion and induce apoptosis by regulating PI3K/Akt, NF-κB, MAPK and other signaling pathways.[25] Our previous study found that AS IV inhibited NPC tumor growth by reducing the expression of SATB2 and inactivating the Wnt signaling pathway.[22] In particular, several studies have suggested that AS IV has the potential to regulate the tumor immune microenvironment. AS IV promotes T cell activation by remodeling tumor microenvironment (TME) and promotes macrophage M1 polarization, thereby enhancing anti-PD-1 therapy and inhibiting tumor growth.[26] However, whether AS IV can affect PD-L1 expressions in tumor via regulating the SATB2/Wnt/β-catenin axis and then reshape the NPC immune microenvironment has not been systematically reported.

This study will validate AS IV's inhibitory effects on PD-L1 expressions in NPC by combining cell experiments with animal models. To clarify SATB2's key mediating roles in this process; to explore its effect on downstream Wnt/β-catenin activity; anti-tumor immune effect of AS IV was comprehensively evaluated from the aspects of T cell activation, killing function and malignant phenotype of tumor cells, so as to provide reference for the immunotherapy of NPC.

Materials and Methods

Cell grouping and intervention

Human immortalized nasopharyngeal epithelial cells NP-69 and human NPC cells C666-1 and HK-1 were purchased from Sunncell Biotechnology Co., Ltd., Wuhan, China (SNL-565, SNL-516, SNL-563). The above cells were seeded in DMEM complete medium (SNM-001E, SUNNCELL) containing 10% fetal bovine serum (FBS) and 1% penicillin-streptomycin, and cultured in a

37℃, 5% CO_2 cell incubator (3111; ThermoFisher Scientific, Waltham, MA, USA). Passage was performed when the cells were fused to 80%.

SiSATB2, OE-SATB2 and related negative controls were purchased from Sangon Biotechnology Co., Ltd. (Shanghai, China). C666-1 and HK-1 cells (1×10^5 cells/well) were seeded in plates, and transfected when the cell fusion degree reached 70%. The complete medium without double antibody was replaced 2 h before transfection. Following LipofectamineTM 3000 transfection (L3000001; Invitrogen, Austin, TX, USA) instruction, siSATB2 and OE-SATB2 were diluted in 25 µL Lipofectamine 3000, incubated for 15 min to form a complex, and then evenly added. After transfection for 6 h, the cells were replaced with fresh complete medium and cultured for 48 h. SATB2 protein expressions were assessed using Western blot to verify the transfection efficiency. C666-1 and HK-1 cells were seeded in plates (1.5×10^4 cells/well). The cells were treated with 100, 200 and 400 µM AS IV (HY-N0431, MedChemExpress, Monmouth Junction, NJ, USA), 5 µg/mL Atezolizumab (HY-P9904, MedChemExpress) and 100 ng/mL Wnt pathway inhibitor DKK-1 (HY-P72968, MedChemExpress) for 24 h.[22]

Dual-luciferase reporter assay

The PD-L1 promoter (GenBank accession number: NM_001314029.1) was amplified by PCR using nasopharyngeal epithelial cell genomic DNA as a template and cloned into pGL3-Basic Vector (E1081; Promega, Madison, WI, USA). Specific point mutations were introduced by overlapping PCR extension using the full-length promoter as a template. Subsequently, the constructed PD-L1 promoter reporter plasmid, pGL3-Basic empty vector (as a negative control) and the Renilla luciferase reporter plasmid (as an internal reference) were co-transfected into C666-1 and HK-1 cells using LipofectamineTM 3000 transfection reagent. After 48 h of transfection, the cells were treated with fresh complete medium containing 100, 200 and 400 µM AS IV for 24 h. After the treatment, the cells were collected and lysed with lysis buffer, and the supernatant was centrifuged. The activity of firefly luciferease and Renilla luciferase was measured using a multifunctional microplate reader (1410101; ThermoFisher Scientific) in strict accordance with the operation procedure of the dual luciferase reporter gene assay kit (E1081; Promega). Three independent replicates were set in each concentration group, and Renilla luciferase activity was used as an internal reference to standardize the luciferase activity driven by the PD-L1 promoter. The luciferase activity of the empty vector control group did not change significantly under different concentrations of AS IV treatment.

RT-qPCR

RNAiso Plus reagent (9108Q; TaKaRa, Tokyo, Japan) extracted total RNA from C666-1 and HK-1 cells, and the concentration and purity of RNA were determined by an ultramicro nucleic acid protein analyzer (Q5000; Quawell Technology Inc., San Jose, CA, USA). Reverse transcription reaction was performed according to HiScript III All-in-one RT SuperMix Perfect for qPCR (R333-01; Vazyme, Nanjing, China). According to the HiScript II One Step RT-PCR Kit (P611-01; Vazyme), RT-PCR reaction was performed on a PCR instrument (StepOne; Applied Biosystems, Waltham, MA, USA). The CT values of each hole were recorded. GAPDH served as the reference gene, and PD-L1 mRNA expression was analyzed by the $2^{-\Delta\Delta CT}$ method. All primer sequences: PD-L1: F: CAATTTGTGCATGGAGAGGAAG, R: GTTGTATGGGGCATTGACTTTC; GAPDH: F: GCATTGCCCTCAACGACCAC, R: CCACCACCCTGTTGCTGTAG.

Cell co-culture

Peripheral blood mononuclear cells (PBMCs) were isolated from 10 mL of human peripheral blood by Ficoll density gradient centrifugation. According to the human $CD8^+$ T cell sorting kit (70909-50; BEAVER, Suzhou, China), 300 µL of sorting buffer was added to re-suspend PBMCs, and $CD8^+$ T cell sorting magnetic beads were added. The cells were incubated for 30 min, then placed on a magnetic rack for 8 min, and resuspended in medium containing 10% FBS and 100 U/mL Interleukin-2 (IL-2). Then they were inoculated into 24-well plates coated with CD3 (2.5 µg/mL) and CD28 (2 µg/mL) antibodies and cultured in a cell incubator for 72 h to amplify $CD8^+$ T cells. $CD8^+$ T cells were co-cultured with C666-1 and HK-1 cells at a ratio of 10:1 for 48 h.

Cytotoxicity test

$CD8^+$ T cell killing effect on NPC cells was detected according to the cytotoxicity kit (C20301; ThermoFisher Scientific). Ten µL of lactate dehydrogenase (LDH) release reagent was added to each well and incubated for 30 min. The supernatant was collected by centrifugation, and the absorbance (A) value of the supernatant at 490 nm was detected by microplate reader.

Flow cytometry experiment

The $CD8^+$ T cells in the co-incubation system were resuspended in 100 µL PBS solution and incubated with 1 µL PD-1-FITC (E-AB-F1229C; Elabscience, Wuhan, China) antibody at 4°C for 30 min. After washing, the cells were resuspended in 500 µL PBS. PD-1 expressions was analyzed using flow cytometry (BD FACSCaliburTM; BD biosciences, San Jose, CA, USA).

CCK-8 assay

Ten µL of CCK-8 reagent (96992; Sigma-Aldrich, St. Louis, MO, USA) was added to each well of C666-1 and HK-1 cells in the co-culture system and incubated (37°C, 2 h). The $A_{450\ nm}$ value was detected to evaluate the proliferation activity of NPC cells, so as to indirectly reflect the killing efficiency of T cells. At the same time, after NP-69 cells were treated with 100, 200 and 400 µM AS IV for 24 h, CCK-8 reagent was added to detect, and $A_{450\ nm}$ value was detected by the microplate reader to evaluate the relative viability of cells.

Plate cloning experiment

C666-1 and HK-1 cells were seeded into dishes containing complete medium (2 mL). In order to evenly distribute the cells, the culture dish was slowly rotated for 1 min after the cells were inoculated. After the cells were adherent, co-culture or reagent intervention was performed. The cell growth state and density were observed during the culture process, and the medium was replaced every two days. Cell colonies larger than 50 µm in diameter were visible to the naked eye under a microscope (XK-DZ004; SINICO Optical Instrument Co., LTD, Shenzhen, China). After 14 days, the cells were fixed with 4% paraformaldehyde (HY-Y0333; MedChemExpress) for 20 min and stained with 0.1% crystal violet (32675; Sigma-Aldrich) for 10 min. Finally, the excess dye was gently washed with running water and the culture dish was dried at room temperature. Then the colony formation of cells was observed under a microscope.

Transwell experiment

After thawing (4°C), Matrigel (HY-K6002;MedChemExpress) was diluted with serum-free medium at a ratio of 1:8, and 100 µL of diluted Matrigel was evenly inoculated into the upper chamber. The gel was formed when standing (37°C) for 0.5-1 h. C666-1 and

HK-1 cells (4×10^4 cells/well) were inoculated into 100 μL serum-free medium in the upper chamber, and 500 μL medium containing 20% FBS was added to the lower chamber. The cells remaining on the upper surface of the chamber after incubation at 37°C for 48 h were erased with cotton swabs, and the cells on the lower surface of the upper chamber were invasive cells. The cells that invaded the lower surface of the upper chamber were fixed with 4% paraformaldehyde for 30 min and stained with 0.1% crystal violet for 10 min. After washing the crystal violet staining solution, the cells were naturally dried in a ventilated place for 2 h. Invasive cells were counted under the microscope. The cell migration experiment was performed directly using a chamber not covered with Matrigel, and the remaining experimental steps were consistent.

Cell scratch test

When the density of C666-1 and HK-1 cells (2×10^6 cells/well) in the co-culture system was close to 100%, and 100 μL pipette tips were used to scratch the plate. The cells were incubated with medium containing different doses of COP for 24 h. The scratch area was photographed by microscope at 0 h and 24 h, and the cell migration of each group was observed. Image J software was used to measure and record the relative migration rate of cells. Relative migration rate = (0 h scratch width-24 h scratch width) / 0 h scratch width.

Mouse xenograft model

SPF grade huHSC-NCG mice, 4-6 weeks of age, weighing 15-18 g, were purchased from self-collection Yaokang Biotechnology Co., Ltd. (Jiangsu, China). The huHSC-NCG model is a fully humanized immune system mouse constructed by transplanting human umbilical cord blood-derived $CD34^+$ hematopoietic stem cells into NCG mice. All mice were housed in an SPF animal room with a temperature of 22°C and a relative humidity of 50% to simulate normal circadian rhythms. Mice can eat and drink freely. The experiment was carried out after 1 week of adaptive feeding. The related research has been approved by the The First Affiliated Hospital of Hainan Medical University Ethics Committee.

The mice were randomly divided into a control group, a 40 mg/kg AS IV treatment group, an aPD-L1 group and a 40 mg/kg AS IV+aPD-L1 treatment group, with 9 mice in each group. 0.2 mL of C666-1 cells (1×10^7 cells/mL) were inoculated subcutaneously into mice to construct a mouse xenograft model. After 3 days, the mice were given 40 mg/kg AS IV (0.3 mL) and/or intraperitoneal injection of 100 mg aPD-L1 (BE0146 l; Bioxcell, West Lebanon, NH, USA) daily for 12 days.[27] During the experiment, the long diameter and short diameter of the tumor were measured every 3 days, and the tumor volume = 1/2 × length × $width^2$ was calculated. Subsequently, the mice were anesthetized with 1% pentobarbital sodium and sacrificed. The tumor tissue was stripped, its weight was measured, and photographs were taken. Some of the tumor tissues were immersed in 4% paraformaldehyde for fixation. Another portion of the tumor tissue was stored at -80°C for subsequent experiments.

TUNEL staining

The fixed subcutaneous tumor tissue of mice was dehydrated by gradient ethanol, transparent by xylene and embedded in paraffin, and serially sliced with a slicer (RM2255; Leica, Wetzlar, Germany), with a thickness of about 5 μm. Subsequently, paraffin sections were subjected to dewaxing to water, DNase-free protease K (20 μg/mL, ST532; Beyotime) to repair antigens, and membrane rupture. C666-1 and HK-1 cells in the co-culture system were collected, fixed with 4% paraformaldehyde, and treated with permeabilized solution. The sections were added with TUNEL reaction solution (C1086; Beyotime) and incubated at 37°C for 1.5 h. The nuclei were re-stained with DAPI (C0060; Solarbio, Beijing, China) for 10 min. The staining was observed under a fluorescence microscope (IX73; Olympus, Tokyo, Japan), and the proportion of positive cells was counted to statistically analyze the apoptosis level of tumor cells and tissues in each group.

Ki-67 immunohistochemistry

After the paraffin sections of subcutaneous tumor tissue were baked, xylene (247642; Sigma-Aldrich) was dewaxed and hydrated with gradient ethanol. After incubation with 3% H_2O_2 for 25 min in the dark, endogenous peroxidase was inhibited. After washing with PBS, the sections were placed in bovine serum albumin (BSA, 5%, V900933; Sigma-Aldrich) for 30 min. Add Ki-67 (ab15580, 1:100; Abcam, Cambridge, UK) primary antibody and refrigerate at 4°C overnight. The next day, the first antibody was discarded, PBS was washed, the second antibody (ab6728, 1:2000; Abcam) was incubated for 2 h, PBS rinsed, DAB (DA1010; Solarbio) coloration, hematoxylin nuclear re-staining. Gradient ethanol dehydration, xylene transparent after sealing. Six fields of view were randomly selected under the microscope to take photos and perform data statistics.

Western blot

The tumor tissues and C666-1 and HK-1 cells were collected and washed with pre-cooled (4°C) PBS, and RIPA reagent (P0013B; Beyotime, Shanghai, China) supplemented with protease inhibitor mixture was added to lyse the cells. After incubation on ice for 30 min, the cells were centrifuged (4°C, 12000 r/min, 15 min), and the supernatant was the total protein. The protein was quantified by a BCA protein assay kit (P0010; Beyotime) and then boiled at high temperature. Proteins were separated using a 12% SDS-PAGE gel and transferred to activated PVDF membranes. After blocking with 5% skim milk for 2 h, the primary antibody (4°C, overnight) was incubated, and the transition condition (37°C, 2 h) was continued to incubate the secondary antibody. The ECL luminescent liquid (HY-K1005, MedChemExpress) was used to enhance the fluorescence signal, and the gel imaging system (iBright CL1500, Invitrogen) detected protein bands. ImageJ software analyzed gray values. GAPDH was used as an internal control to compute different protein expressions. In addition, the nuclear protein and cytoplasmic protein extraction kit (P0028; Beyotime) extracted nuclear protein, and Lamin B1 was used as the internal reference of nuclear protein.

The primary antibody used in this study: PD-L1 (DF6526, 1:2000; Affinity, Jiangsu, China), Perforin (ab261727, 1:1000; Abcam), Granzyme B (ab255868, 1:1000; Abcam), SATB2 (ab34735, 1:00; Abcam), β-catenin (ab68183, 1:1000; Abcam), cellular-myelocytomatosis viral oncogene homolog (c-MYC, ab168727, :1000; Abcam), Axin2 (DF6978, 1:2000; Affinity), Lamin B1 (ab133741, 1:10000; Abcam), and GAPDH (ab181602, 1:10000; Abcam).

ELISA

Interferon-γ (IFN-γ) levels were detected according to ELISA detection kits (E-EL-H0108; Elabscience, Wuhan, China). The tumor tissues were homogenized with normal saline, and the supernatant was collected after centrifugation. The supernatant of co-culture of cells in each group was collected, coated with antigen, blocked with blocking solution, added with standard substance and sample to be tested, enzyme-labeled antibody, color development solution, termination solution to terminate the reaction, and the A value was detected by microplate reader. A standard curve was drawn to measure IFN-γ level in the supernatant of each

group.

Flow cytometry of tumor tissue

Freshly peeled tumor tissues were washed with PBS to remove bloodstains, cut into small pieces of about 1-2 mm^3, added with RPMI 1640 medium containing 0.5 mg/mL collagenase IV (C8160; Solarbio) and 0.1 mg/mL DNase I (D8071; Solarbio), and digested in a shaker at 37°C for 30 min. The digested cell suspension was filtered through a 70 μm cell sieve, the filtrate was collected, centrifuged for 5 min, and the supernatant was discarded. After washing with PBS, the cell precipitate was resuspended in 100 μL PBS and incubated with 1 μL APC anti-human CD8 antibody (E-AB-F1110E; Elabscience) at 4°C for 30 min in the dark. After washing, the cells were resuspended in 500 μL PBS, and the number and proportion of $CD8^+$ T cells in tumor tissues were detected by flow cytometry. FlowJo software was used for data analysis.

Chromatin immunoprecipitation (ChIP)-qPCR

C666-1 and HK-1 cells were collected, formaldehyde was added to the final concentration of 1%, and cross-linked at room temperature for 10 min. The intracellular protein and DNA complexes were fixed, and the cells were lysed after glycine termination. The chromatin was fragmented to 200-600 bp using an ultrasonic disruptor. The supernatant was used as an Input control, and the remaining samples were incubated with 2 μg of β-catenin antibody (8480; Cell Signaling Technology, Danvers, MA, USA) or normal rabbit IgG (2729; Cell Signaling Technology) as a negative control at 4°C overnight. The next day, protein A/G magnetic beads were added for incubation for 2 h. After enrichment by magnetic frame, the magnetic beads were washed with low-salt and high-salt washing buffer in turn. Elution buffer (containing 1% SDS, 0.1 M $NaHCO_3$) and protease K (PI810; Beyotime) were added and decrosslinked overnight at 65°C. The purified DNA was used to amplify the PD-L1 promoter region by PCR. The primer sequences for the PD-L1 promoter were 5′-ATGTAGCTCGGGATGGGAAGT-3′ (forward) and 5′-TGTGTGTGTGTGTATGGGTGTA-3′ (reverse). With Input as the internal reference, the relative enrichment level of β-catenin in the PD-L1 promoter region was calculated by the percentage input method (% input).

Statistical analysis

Statistical analysis of the data was conducted using SPSS 27.0 software. All data were subjected to normality and homogeneity of variance tests. Each group's data was presented as the mean ±SD. The Student's *t*-test was used for pairwise comparisons between two groups, and One-way ANOVA analysis along with the Tukey *post-hoc* test was employed for comparisons among multiple groups. A *p*-value <0.05 was considered statistically significant.

Results

AS IV down-regulated PD-L1 expressions

PD-L1 binds to PD-1 to suppress T cell activity, induce T cell senescence, and then complete tumor immune escape.[28,29] We first evaluated the cytotoxicity of AS IV on normal nasopharyngeal epithelial cells NP-69. There was no significant difference in the viability of NP-69 cells treated with AS IV (Figure 1A), indicating that AS IV in this concentration range had no obvious toxic effect on normal cells and had good *in vitro* safety. Subsequently, to further investigate whether AS IV could regulate PD-L1, C666-1 and HK-1 cells were transfected with a luciferase reporter plasmid con-

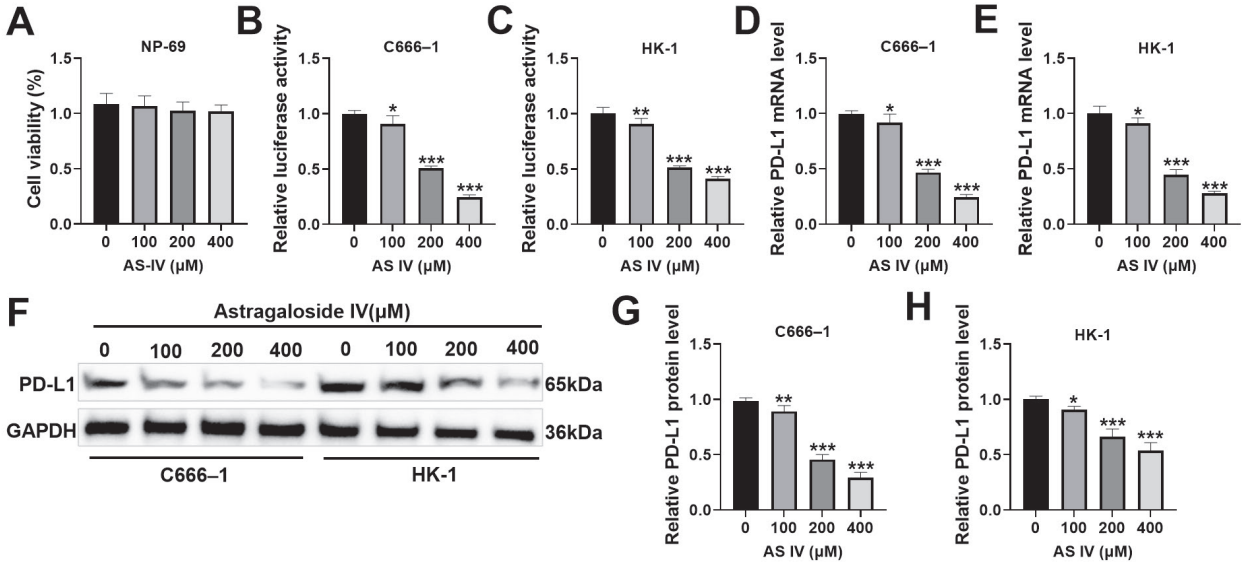

Figure 1. AS IV down-regulated PD-L1 expression. **A**) CCK-8 assay was used to detect the effect of 100, 200 and 400 μM AS IV on the viability of NP-69 cells. **B,C**) NPC cells were co-transfected with a luciferase reporter plasmid containing the PD-L1 promoter and treated with AS IV for 24 h; luciferase activity was determined by dual luciferase reporter system; AS IV markedly reduced the luciferase activity driven by the PD-L1 promoter. **D,E**) PD-L1 mRNA expressions were assessed through RT-qPCR, which was significantly decreased after AS IV intervention. F-H) Western blot detected PD-L1 protein levels, which were significantly reduced after AS IV intervention. n=6; **p*<0.05, ***p*<0.01, ****p*<0.001 *vs* 0 group.

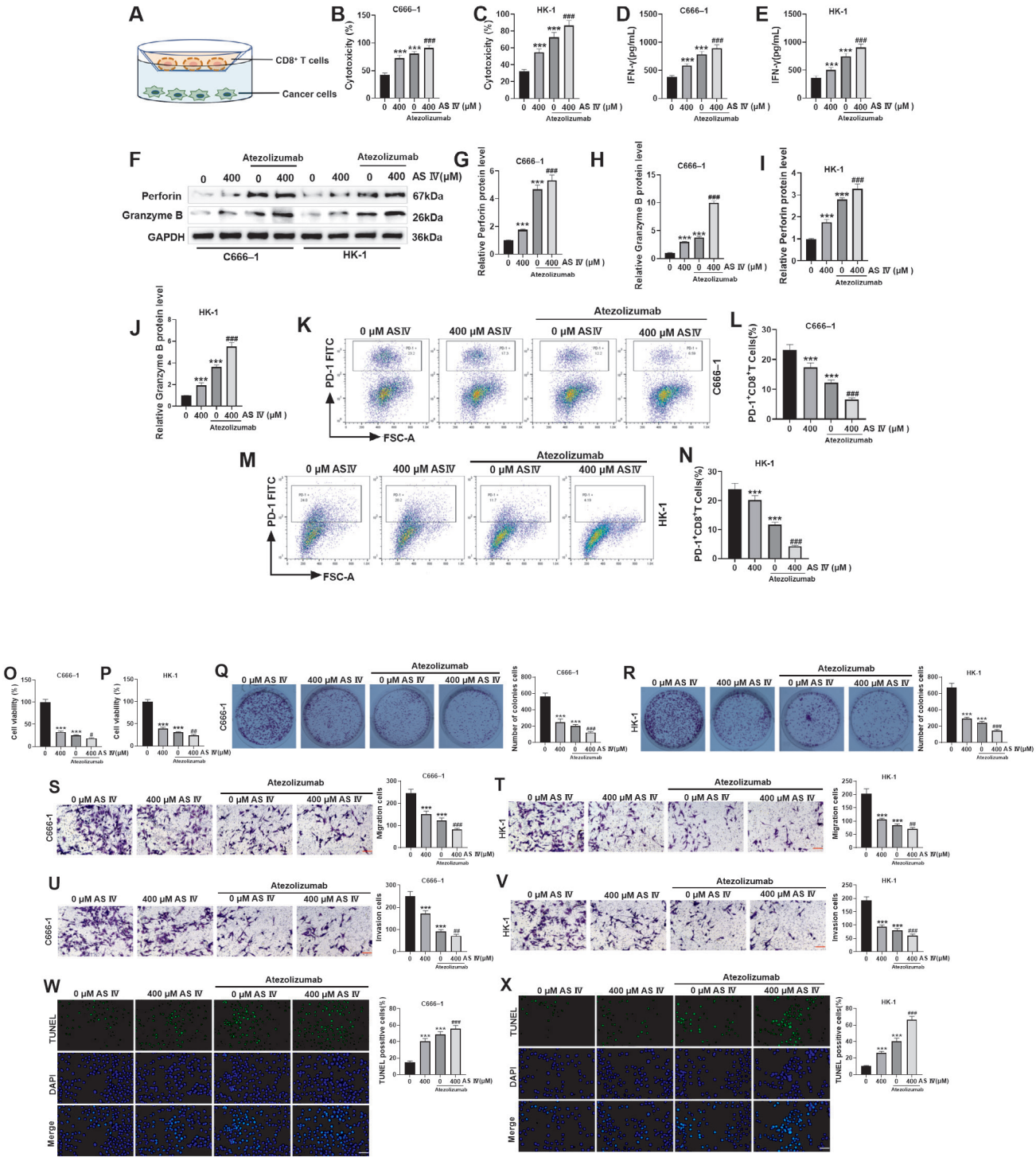

Figure 2. AS IV enhanced CD8⁺ T cell killing activity and inhibited NPC cell malignant progression. **A**) Schematic diagram of co-culture of C666-1 and HK-1 cells with CD8⁺ T cells. **B,C**) LDH assay measured CD8⁺ T cell cytotoxicity after co-culture, which was significantly increased after AS IV intervention. **D,E**) The content of IFN-γ was measured using ELISA, which was significantly increased after AS IV intervention. **F-J)** Western blot detected the protein levels of Perforin and Granzyme B, markers of CD8⁺ T cell activation, which were significantly increased after AS IV intervention. **K-N**) PD-1 positive cells were measured using flow cytometry. AS IV significantly reduced PD-1 expression proportion. **O,P**) CCK-8 detected NPC cell proliferation after co-culture; AS IV significantly reduced cell viability. **Q,R**) Plate cloning assay detected the proliferation of tumor cells; AS IV significantly reduced the number of cloned cells. **S-V**) Transwell detected tumor cell migration and invasion abilities after co-culture, which was significantly reduced after AS IV intervention (×20, 100 μm). **W,X**) TUNEL staining detected tumor cell apoptosis level after co-culture; AS IV significantly raised TUNEL-positive cell numbers (×40, 50 μm). n=6; ***p<0.001 *vs* 0 group; $^{\#}p$<0.05, $^{\#\#}p$<0.01, $^{\#\#\#}p$<0.001 *vs* 0+Atezolizumab group.

taining the PD-L1 promoter and treated with 100, 200 and 400 μM AS IV. AS IV significantly reduced the luciferase activity driven by the PD-L1 promoter, and these inhibitory effects were enhanced with increasing AS IV concentration (Figure 1 B,C). Moreover, PD-L1 levels were significantly decreased with the increase of AS IV concentration (Figure 1 D-H). These results together demonstrated that AS IV effectively suppressed PD-L1 expressions in NPC.

AS IV down-regulated PD-L1 expressions in NPC, increased CD8$^+$ T cell killing activity and inhibited NPC cell malignant progression

We extracted CD8$^+$ T cells and co-cultured them with C666-1 and HK-1 cells for 48 h, and intervened with AS IV and PD-L1 blocking antibody Atezolizumab. The co-culture diagram was shown in Figure 2A. Subsequently, CD8$^+$ T cells were collected. The LDH release assay showed that AS IV significantly increased LDH release (Figure 2 B,C), indicating that the direct killing ability of T cells was enhanced. ELISA showed that IFN-γ content was significantly increased after AS IV intervention (Figure 2 D,E), suggesting that T cells were widely activated. The combined use of Atezolizumab further increased LDH release and IFN-γ levels. Perforin and Granzyme B expressions were markedly enhanced (Figure 2 F-J). Furthermore, the proportion of PD-1 positive cells decreased significantly after AS IV intervention, and further decreased in AS IV+Atezolizumab intervention (Figure 2 K-N). These data together demonstrated that AS IV intervention enhanced CD8$^+$ T cell activity and cytotoxicity and produced synergistic effects with PD-L1 blocking antibody Atezolizumab.

Subsequently, C666-1 and HK-1 cells were collected. AS IV intervention markedly inhibited the growth and colony formation abilities of tumor cells when co-cultured with T cells (Figure 2 O-R), and the combined use of Atezolizumab could produce a stronger synergistic inhibitory effect. This indicated that inhibition of PD-L1 expression further released the killing potential of T cells activated by AS IV. In addition, AS IV and Atezolizumab intervention markedly weakened tumor cell migration and invasion abilities (Figure 2 S-V) and induced apoptosis (Figure 2 W-X). In summary, AS IV down-regulated PD-L1 expressions in NPC, activated CD8$^+$ T cells, enhanced its tumor killing toxicity, inhibited NPC cell malignant progression, and had a synergistic effect with PD-L1 blocking antibody Atezolizumab.

Inhibiting the SATB2/Wnt/β-catenin axis inhibited PD-L1 expression

The Wnt/β-catenin axis is an essential driver of tumors.[30] SATB2 expression was markedly decreased after transfection with siSATB2 (Figure 3 A,B), and significantly increased after transfection with OE-SATB2 (Figure 3 G,H). The cell model of SATB2 stable knockdown and overexpression was successfully constructed. In SATB2-knockdown cells, the total β-catenin protein and its

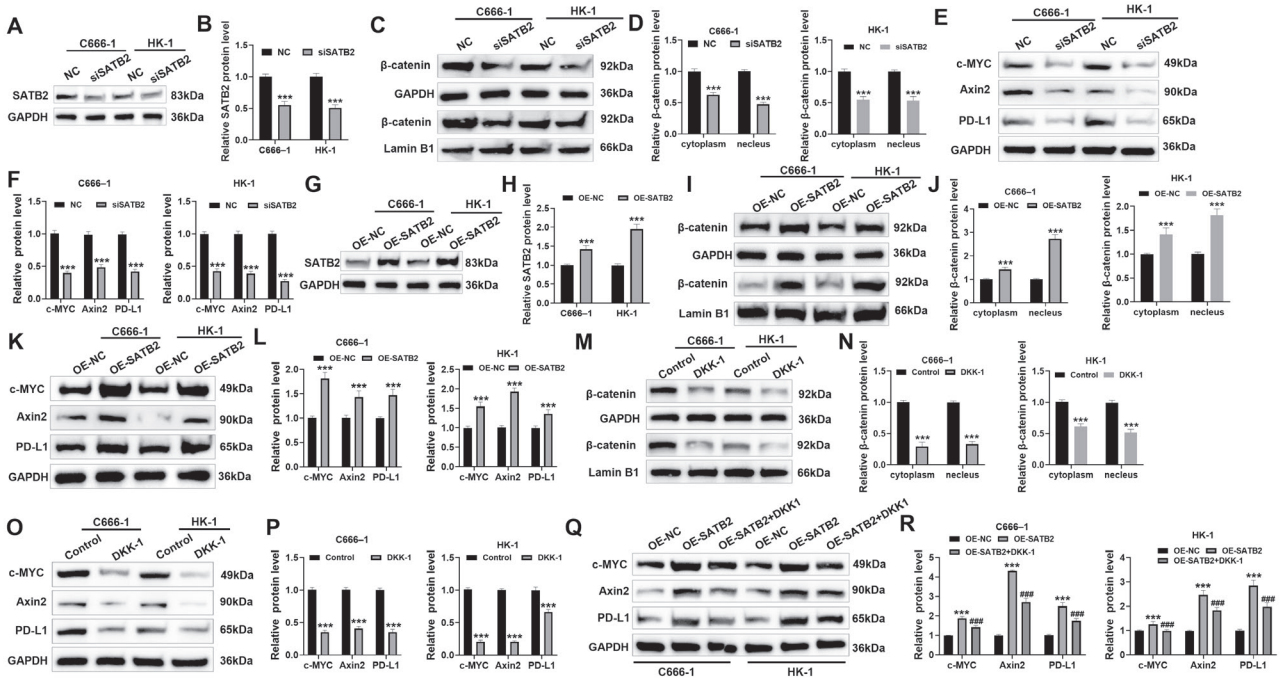

Figure 3. Inhibiting SATB2/Wnt/β-catenin axis inhibited PD-L1 expression. **A,B**) siSATB2 was transfected into NPC cells; the level of SATB2 protein was detected by WB, which was significantly reduced after transfection of siSATB2. **C-F**) Western blot detected Wnt/β-catenin pathway and PD-L1 protein levels; SATB2 knockdown significantly reduced the total β-catenin protein and its nuclear levels, and reduced c-MYC, Axin2 and PD-L1 proteins. **G,H**) OE-SATB2 was transfected into NPC cells; the level of SATB2 protein was detected by WB, which was significantly increased after transfection of OE-SATB2. **I-L**) Western blot detected Wnt/β-catenin pathway and PD-L1 protein levels; SATB2 overexpression significantly increased c-MYC, Axin2, PD-L1, total β-catenin protein and its nuclear level. **M-P**) C666-1 and HK-1 cells were treated with Wnt inhibitor DKK-1; Western blot detected Wnt/β-catenin pathway and PD-L1 protein levels; DKK-1 significantly reduced c-MYC, Axin2, PD-L1, total β-catenin protein and its nuclear level. **Q,R**) SATB2 overexpressing cells were treated with DKK-1. c-MYC, Axin2 and PD-L1 proteins were detected using Western blot, which were significantly decreased after DKK-1 treatment. n=6; ***p<0.001 *vs* NC/OE-NC/Control group; $^{###}p$<0.001 *vs* OE-SATB2 group.

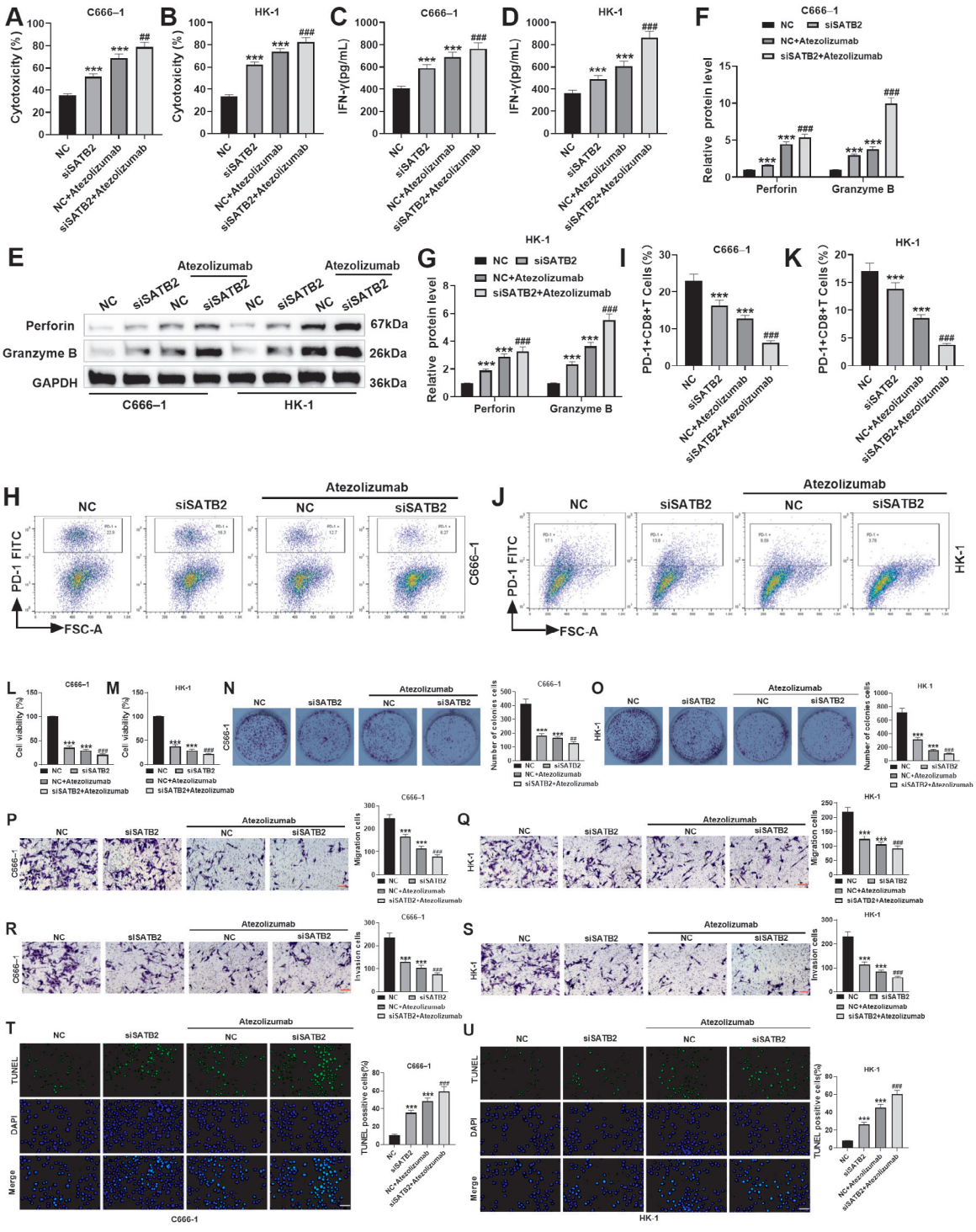

Figure 4. . SATB2 knockdown enhanced CD8⁺ T cell killing activity and inhibited NPC cell malignant phenotype. **A,B**) LDH assay measured CD8⁺ T cell cytotoxicity after co-culture, which increased significantly after SATB2 knockdown. **C,D**) The content of IFN-γ was measured through ELISA, which was significantly increased after SATB2 knockdown. **E-G**) Western blot detected the protein levels of Perforin and Granzyme B, markers of CD8⁺ T cell activation, which increased significantly after SATB2 knockdown. **H-K**) PD-1 positive cells were detected by flow cytometry; SATB2 knockdown significantly reduced PD-1 expression. n=6, ***p<0.001 *vs* NC group; ##p<0.01, ###p<0.001 *vs* NC+Atezolizumab group. **L,M**) CCK-8 detected cell proliferation after co-culture; SATB2 knockdown significantly reduced cell viability. **N,O**) Plate cloning assay detected the proliferation of tumor cells; SATB2 knockdown significantly reduced the number of cloned cells. **P-S**) Transwell assays detected tumor cell migration and invasion abilities after co-culture, which was significantly reduced after SATB2 knockdown (×20, 100 μm). **T,U**) TUNEL staining detected the apoptosis level of tumor cells after co-culture. SATB2 knockdown significantly elevated TUNEL-positive cell numbers (×40, 50 μm). n=6, ***p<0.001 *vs* 0 group; ##p<0.01, ###p<0.001 *vs* 0+Atezolizumab group.

nuclear level were significantly decreased (Figure 3 C,D), and downstream targets c-MYC and Axin2 expressions were also reduced accordingly, while PD-L1 protein was markedly inhibited (Figure 3 E,F). On the contrary, the above protein levels were significantly reversed in SATB2-overexpressing cells (Figure 3 I,L). This positive feedback result proved that SATB2 was an essential upstream regulator of this pathway, and its expression level determined the activation state of the axis and PD-L1 expressions. Wnt inhibitor DKK-1 treatment inhibited β-catenin activation and c-MYC, Axin2 and PD-L1 expression (Figure 3 M-P), indicating that PD-L1 expression was dependent on Wnt/β-catenin pathway activity. Concurrently, DKK-1 reversed the up-regulation of these molecules induced by SATB2 overexpression (Figure 3 Q,R), suggesting that the up-regulation of PD-L1 by SATB2 might be achieved by activating this pathway. In conclusion, inhibition of the SATB2/Wnt/β-catenin axis reduced PD-L1 expression.

Inhibition of the SATB2/Wnt/β-catenin signaling axis improved the immune killing effect by inhibiting PD-L1 expression

In the co-culture system of SATB2 knockdown tumor cells and $CD8^+$ T cells, LDH release and IFN-γ secretion were markedly increased (Figure 4 A,D), and the combined use of Atezolizumab further amplified this enhancement effect. WB results further showed that Perforin and Granzyme B protein levels were significantly increased after SATB2 knockdown, and further increased after siSATB2+Atezolizumab treatment (Figure 4 E-G). At the same time, flow cytometry found that PD-1 positive rate, a surface depletion marker, was markedly lessened with siSATB2 tumor cells (Figure 4 H-K), and the combined use of Atezolizumab further alleviated T cell functional inhibition. Knockdown of SATB2 promoted $CD8^+$ T cell activity and function.

It was found that SATB2 knockdown could significantly inhibit the proliferation (Figure 4 L,M), colony formation (Figure 4 N,O), migration and invasion (Figure 4 P-S) of tumor cells when co-cultured with T cells, and induce apoptosis of NPC cells (Figure 4 T,U), suggesting that knockdown of SATB2 could inhibit the malignant phenotype of NPC. It was worth noting that the combined use of Atezolizumab further amplified this inhibitory effect, resulting in a synergistic enhanced killing effect. In summary, targeted inhibition of SATB2 down-regulated PD-L1 expression by blocking the Wnt/β-catenin signaling axis, thereby activating $CD8^+$ T cells and their killing ability to NPC cells, and inhibiting NPC malignant phenotype.

AS IV inhibited SATB2/Wnt/β-catenin signaling axis activation and down-regulated PD-L1 expression

After C666-1 and HK-1 cells were treated with AS IV, the total protein and nuclear levels of SATB2 and β-catenin were significantly inhibited, and downstream key targets c-MYC and Axin2 protein also decreased, suggesting that the SATB2/Wnt/β-catenin axis was suppressed; PD-L1 protein level was also significantly decreased (Figure 5 A-D). We used ChIP-PCR to detect the enrichment of β-catenin in the PD-L1 promoter region. There was no significant enrichment in the PD-L1 promoter region when using IgG antibody for immunoprecipitation; after immunoprecipitation with β-catenin antibody, the enrichment level of the PD-L1 promoter region was significantly increased, indicating that β-catenin could directly bind to the PD-L1 promoter. After AS IV treatment, the binding enrichment level of β-catenin in the PD-L1 promoter region was significantly reduced (Figure 5E), confirming that AS IV could block the binding of β-catenin to the PD-L1 promoter. While treated with 400 μM AS IV, overexpression of SATB2 significantly increased SATB2, β-catenin, c-MYC, Axin2 and PD-L1 expressions (Figure 5 F-I), partially reversing the inhibitory effect of AS IV on these molecules. In summary, AS IV suppressed the SATB2/Wnt/β-catenin axis, resulting in reduced PD-L1 expression.

AS IV inhibited tumor progression in tumor-bearing mice by down-regulating the SATB2/Wnt pathway and inhibiting PD-L1 expression

After that, we conducted *in vivo* experiments. The tumor growth curve, tumor volume and final tumor weight of the AS IV treatment group showed a significant decrease (Figure 6 A-C). When AS IV intervention, TUNEL positive cells in tumor tissues enhanced markedly (Figure 6 D,E), and the positive rate of proliferation marker Ki-67 decreased (Figure 6 F,G), which confirmed that AS IV could inhibit tumor cell growth. AS IV treatment also significantly reduced SATB2, β-catenin, c-MYC, Axin2 and PD-L1 expressions in tumor tissues (Figure 6 H,I). Secondly, the number of infiltrating $CD8^+$ T cells raised (Figure 6 J,K), and the levels of Perforin and Granzyme B protein increased significantly (Figure 6 L,M), indicating that $CD8^+$ T cells were highly activated. And AS IV significantly increased IFN-γ content in the blood (Figure 6N). In addition, in the AS IV+aPD-L1 combined treatment group, SATB2/Wnt/β-catenin pathway and PD-L1 protein expressions were inhibited to their lowest level, and the immune response was maximized and activated, showing a significant synergistic anti-tumor effect. In summary, AS IV down-regulated PD-L1 expression by targeting the SATB2/Wnt/β-catenin pathway, thereby reshaping the immune microenvironment and increasing $CD8^+$ T cell activity, and ultimately achieving the effect of inhibiting tumor growth.

Discussion

As a malignant tumor with unique geographical and etiological characteristics, the treatment of NPC faces severe challenges in the locally advanced and metastatic stages, especially TME-mediated immunosuppression and immune escape, which has become a key bottleneck restricting the efficacy.[31,32] Tumor immunotherapy has made significant progress in tumor therapy.[33] It is of great significance in PD-L1 in tumor immunotherapy.[34] PD-L1 is an immune checkpoint protein. It can bind to PD-1 receptors, transmit inhibitory signals, cause T cell incompetence, and help tumor cells escape from the surveillance and attack of the immune system. This is one of the key ways for tumor immune escape.

In TME of NPC, PD-L1 is a key factor that impairs T cell activation.[35] $CD8^+$ T cells are the main cytotoxic T lymphocytes in the body, which have a killing effect on tumor cells. The infiltration and activity of $CD8^+$ T cells are essential for tumor immunotherapy.[36] In TME, tumor cells promote immune escape by destroying $CD8^+$ T cell toxic function or inhibiting immune factor contents, including TNFα, IFNγ and Granzyme B by $CD8^+$ T cells.[37,38] An important contribution of this study is that AS IV significantly enhanced the activation (increased secretion of IFN-γ, Perforin and Granzyme B) and cytotoxicity (increased release of LDH) of $CD8^+$ T cells, and reduced PD-1 expressions. This clearly showed that reducing PD-L1 expressions in tumor could effectively relieve its inhibition of T cells, restore its killing potential, and then inhibit the malignant phenotype of NPC cells. *In vivo* experiments further confirmed that AS IV administration not only inhibited tumor growth, but also significantly increased $CD8^+$ T cell infiltration

and activity. This indicated that AS IV could systematically reshape the immune microenvironment conducive to anti-tumor.

Previous studies have found that the mechanism of AS IV inhibiting the malignant progression of NPC involves reducing the expression of SATB2 and inactivating the Wnt signaling pathway.[22] SATB2 is a protein that serves a crucial role within the nucleus.[39] It regulates biological functions through interacting with DNA and regulating the transcription of other genes. SATB2 abnormal expressions are involved in tumor cell growth, invasion and metastasis. SATB2 expression is elevated in malignant tumors and has become a therapeutic target for clinical anti-tumor.[40] Wang *et al.* showed that silencing SATB2 in hepatocellular carcinoma cells could inhibit cell proliferation, accelerate apoptosis, and improve EMT of tumor cells, thereby reducing invasion and migration.[41] Abnormalities in Wnt/β-catenin signaling can affect anti-tumor immune response by affecting the role of T cells.[42,43] Knockdown of SATB2 markedly lessened β-catenin total protein and nuclear level, reduced c-MYC, Axin2 and PD-L1 proteins, and activated $CD8^+$ T cells and their ability to kill NPC cells. Overexpression of SATB2 activated this axis to promote PD-L1 expression and inhibit $CD8^+$ T cell killing ability to NPC cells. In addition, our experiments using Wnt pathway inhibitor DKK-1 showed that blocking the Wnt pathway could rescue PD-L1 upregulation caused by SATB2 overexpression, which established the indispensability of this pathway as a downstream executor of SATB2. Our work confirmed that AS IV inhibited the SATB2/Wnt/β-catenin signaling axis activation and down-regulated PD-L1 expression.

As the main active ingredient of traditional Chinese medicine *Astragalus membranaceus*, the immunomodulatory function of AS IV has received extensive attention in recent years. In the field of tumor immunity, studies have revealed that AS IV reshapes TME

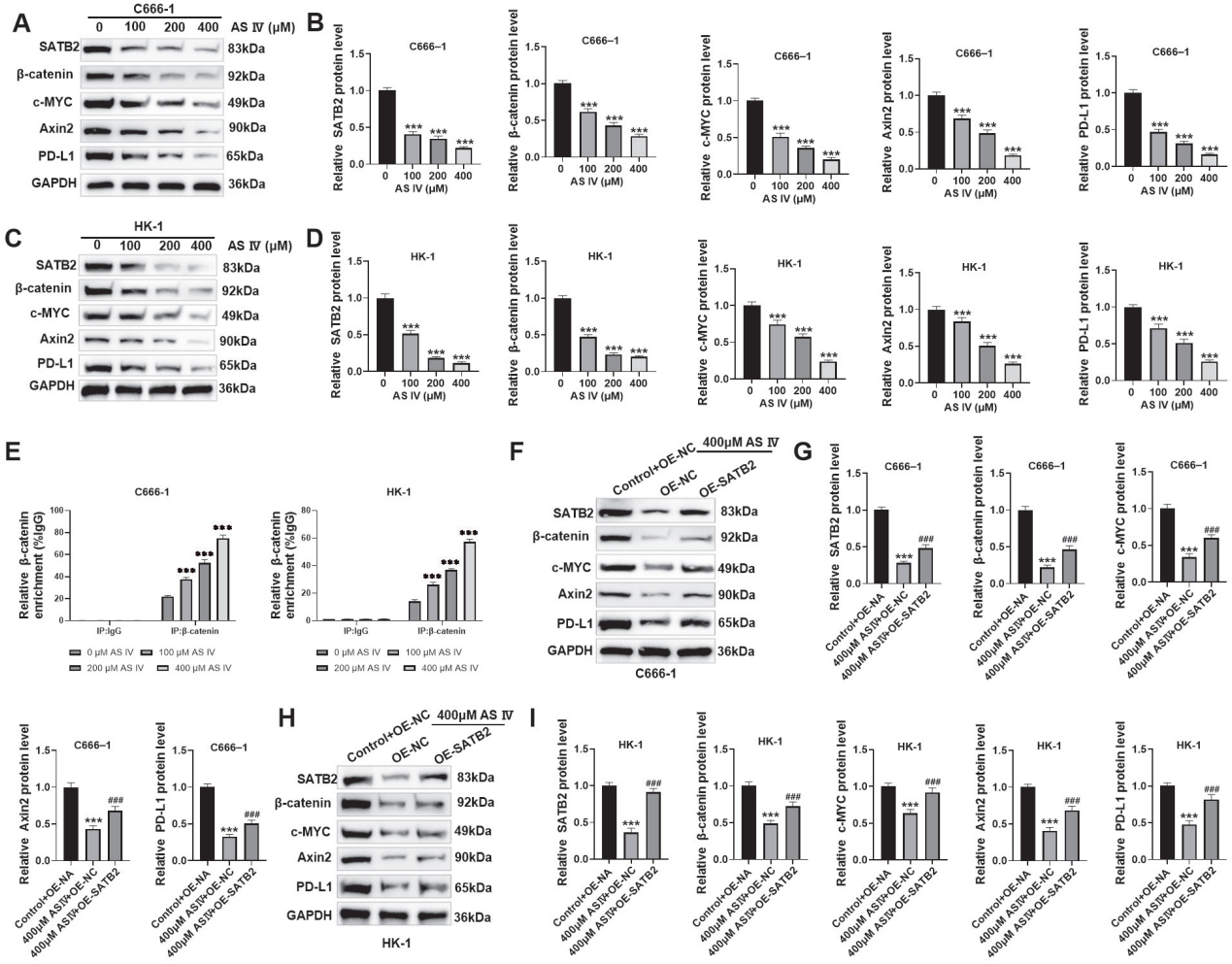

Figure 5. AS IV inhibited SATB2/Wnt/β-catenin signaling axis activation and down-regulated PD-L1 expression. **A-D**) NPC cells were treated with AS IV; Western blot detected SATB2/Wnt/β-catenin pathway and PD-L1 protein level; AS IV significantly reduced the total protein and nuclear levels of SATB2, c-MYC, Axin2, PD-L1, β-catenin. **E**) ChIP-PCR was used to detect the effect of AS IV on the binding enrichment of β-catenin in the PD-L1 promoter region; after AS IV treatment, the binding enrichment level of β-catenin in the PD-L1 promoter region was significantly reduced. **F-I)** SATB2-overexpressing NPC cells were exposed to 400 μM AS IV; Western blot detected SATB2/Wnt/β-catenin pathway and PD-L1 protein levels. SATB2 overexpression significantly increased the total protein and nuclear levels of SATB2, c-MYC, Axin2, PD-L1, β-catenin. n=6; ***p<0.001 *vs* 0/Control+OE-NC group; ###p<0.001 *vs* 400 μM AS IV+OE-NC group.

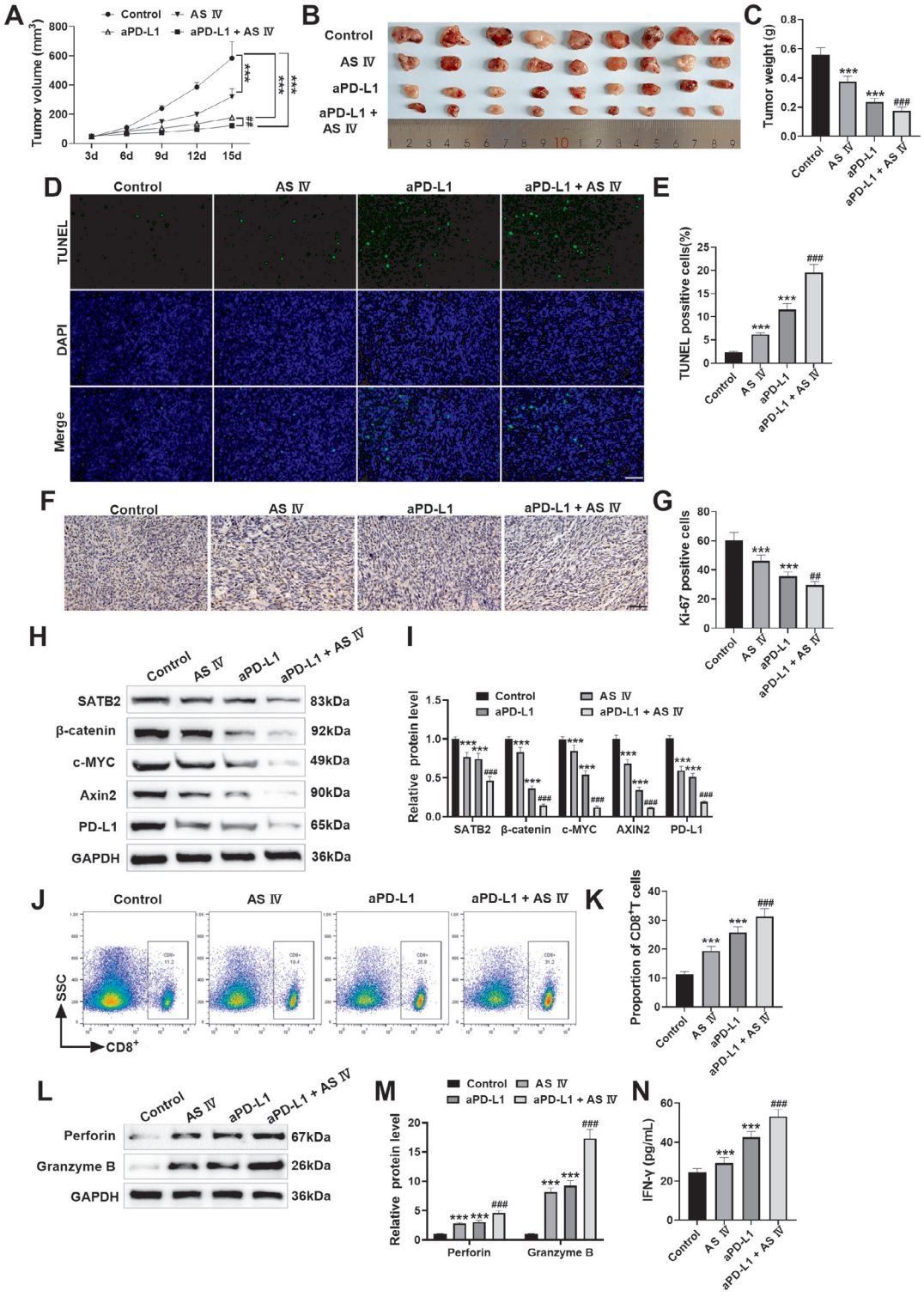

Figure 6. AS IV inhibited tumor progression in tumor-bearing mice by down-regulating SATB2/Wnt pathway and inhibiting PD-L1 expression. **A-C**) Growth curve, morphological image and final tumor weight of subcutaneous tumor; AS IV significantly inhibited tumor growth. **D,E**) TUNEL staining of tumor tissue; AS IV significantly increased the TUNEL positive rate (×40, 50 μm). **F,G**) Immunohistochemistry of tumor tissue; AS IV significantly reduced the positive rate of Ki-67 (×40, 50 μm). **H,I**) Western blot detected SATB2/Wnt/β-catenin pathway and PD-L1 protein levels in tumor tissues; AS IV significantly reduced SATB2, β-catenin, c-MYC, Axin2 and PD-L1 proteins. **J-K**) Flow cytometry detected CD8 expressions; after AS IV intervention, infiltrating $CD8^+$ T cell numbers increased. **L,M**) Western blot detected Perforin and Granzyme B protein expressions, which were markedly increased after AS IV intervention. **N**) IFN-γ contents were detected using ELISA, which increased significantly after AS IV intervention. n=9; ***p<0.001 *vs* Control group; $^{\#\#}p$<0.01, $^{\#\#\#}p$<0.001 *vs* aPD-L1+AS IV group.

through a variety of mechanisms. Liu *et al.* found that AS IV can inhibit epithelial-mesenchymal transition (EMT) and tumor angiogenesis, and affect its downstream target PD-L1 expression by regulating miR-195-5p, a key molecule. High expressions of PD-L are closely associated with tumor immune escape.[44] Ma *et al.* found that AS IV can reduce PD-L1 expressions of Huh-7 and SMMC-7721 cells through the miR-135b-5p/CNDP1 pathway, thereby reducing its related immunosuppression and achieving the inhibition of cell proliferation.[27] Recent studies have also found that AS IV can induce its degradation by directly targeting PPP1R14 B, inhibit the Wnt/β-catenin signaling pathway, and reshape the CX3CL1/$CD8^+$ T cell axis, thereby sensitizing prostate cancer to anti-PD-1 immunotherapy.[45] In bladder cancer, the nano-co-delivery system of AS IV and aPD-L1 has been shown to inhibit NF-κB and STAT3 signaling pathways, increase IFN-γ expression and reduce IL-10 levels, thereby affecting the number and type of tumor-infiltrating T cells.[46] It is worth noting that AS IV has also been found to alleviate influenza-induced inflammatory response in alveolar macrophages by inhibiting the Wnt/β-catenin signaling pathway,[47] suggesting that AS IV has a cross-disease consistency in the regulation of this pathway.

Compared with the above research, this study has made new progress in the following aspects: First, although it has been confirmed that AS IV can down-regulate the expression of PD-L1, its specific regulatory mechanism in NPC is still unclear. We confirmed that AS IV could inhibit the expression of PD-L1 in NPC at the transcriptional, mRNA and protein levels, and provided molecular evidence for the direct binding of β-catenin to the PD-L1 promoter by ChIP-PCR. Secondly, this study accurately anchored the role of AS IV to the specific transcriptional regulatory axis of SATB2/Wnt/β-catenin, and verified the key mediating role of SATB2 in AS IV inhibiting PD-L1 expression through gain-of-function and loss-of-function experiments. Thirdly, this study directly evaluated the effect of AS IV on the infiltration and function of human $CD8^+$ T cells *in vivo* by using the huHSC-NCG mouse model, which provided humanized evidence closer to clinical for the immunomodulatory effect of AS IV. Fourthly, this study confirmed that AS IV and aPD-L1 antibody have synergistic effects in the treatment of NPC, suggesting that AS IV may be a potential sensitizer for the treatment of existing immune checkpoint inhibitors, which is highly consistent with the current trend of exploring the combination of natural products and immunotherapy.[48-50]

This study also has some limitations. Firstly, the direct interaction between AS IV and SATB2 protein needs to be further verified by molecular docking, surface plasmon resonance and other techniques. Secondly, the optimal dosage regimen, pharmacokinetic characteristics of AS IV *in vivo*, and its combination strategy with other immunotherapy (such as PD-1 antibody) need to be further studied in preclinical pharmacodynamics. Thirdly, although the huHSC-NCG humanized mouse model is an advanced tool for studying human immune cell-tumor interaction, there are still some limitations: there are individual differences in the chimerism rate of immune reconstitution, and the reconstructed human immune system may not fully present the natural human immune cell composition and functional diversity due to graft-versus-host reaction or thymus microenvironment differences. Therefore, the potential impact of these factors on immune assessment should be considered when interpreting the results. Fourth, the conclusions of this study need to be verified in more NPC cells and patient-derived xenograft models. In addition, it is not clear whether SATB2 directly binds to the PD-L1 promoter region and regulates its transcription. Subsequent experiments such as ChIP-qPCR, dual-luciferase reporter gene assay and EMSA are needed. Finally, the low oral bioavailability of AS IV as a natural product is a major obstacle to clinical transformation. In the future, it is necessary to use formulation improvement strategies (such as nano-delivery systems) to improve its *in vivo* exposure and tumor targeting, and systematically evaluate its potential for combination with immune checkpoint inhibitors.

In summary, this study found that AS IV can inhibit PD-L1 expressions, thereby affecting $CD8^+$ T cell ability to resist NPC cells. The mechanism is that AS IV can inhibit SATB2 expression, inactivate Wnt/β-catenin signaling, and then down-regulate PD-L1 expression, that is, regulate the SATB2/Wnt/PD-L1 signaling axis. This study may provide a new reference for immunotherapy of NPC.

References

1. Huang H, Yao Y, Deng X, Huang Z, Chen Y, Wang Z, et al. Immunotherapy for nasopharyngeal carcinoma: Current status and prospects (Review). Int J Oncol 2023;63:97.
2. Liu J, Zeng Z, Wang D, Qin G. Minimally invasive surgery for early-stage nasopharyngeal carcinoma. J Craniofac Surg 2022;33:e834-7.
3. Sathasivam HP, Chew SYL, Kim WR, Saw CL, Tan LP, Tengku Din T, et al. Nasopharyngeal carcinoma in adolescent patients: A case series. Clin Otolaryngol 2022;47:486-90.
4. Sadri F, Rezaei Z. The multifaceted role of miR-18b in cancer: exploring oncogenic and tumor-suppressive functions. J Cancer Biomol Ther 2024;1:41-57.
5. Howlett J, Hamilton S, Ye A, Jewett D, Riou-Green B, Prisman E, et al. Treatment and outcomes of nasopharyngeal carcinoma in a unique non-endemic population. Oral Oncol 2021;114:105182.
6. Zhou M, Liu B, Shen J. Immunotherapy for hepatocellular carcinoma. Clin Exp Med 2023;23:569-77.
7. Chen J, Zhang D, Yuan Y. Anti-PD-1/PD-L1 immunotherapy in conversion treatment of locally advanced hepatocellular carcinoma. Clin Exp Med 2023;23:579-90.
8. Deng Z, Teng YJ, Zhou Q, Ouyang ZG, Hu YX, Long HP, et al. Shuyu pills inhibit immune escape and enhance chemosensitization in hepatocellular carcinoma. World J Gastrointest Oncol 2021;13:1725-40.
9. Sahinli H, Akyürek N, Yılmaz M, Kandemir O, Duran AO, Kulaçoğlu S, et al. PD-L1 expression in immune cells is a favorable prognostic factor for nasopharyngeal carcinoma. Indian J Cancer 2021;58:561-6.
10. Gondhowiardjo SA, Handoko, Adham M, Rachmadi L, Kodrat H, Tobing DL, et al. Tumor microenvironment predicts local tumor extensiveness in PD-L1 positive nasopharyngeal cancer. PLoS One 2020;15:e0230449.
11. Liu Y, Li N, Guo Y, Zhou Q, Yang Y, Lu J, et al. APLNR inhibited nasopharyngeal carcinoma growth and immune escape by downregulating PD-L1. Int Immunopharmacol 2024;137:112523.
12. Zhou Y, Xu J, Luo H, Meng X, Chen M, Zhu D. Wnt signaling pathway in cancer immunotherapy. Cancer Lett 2022;525:84-96.
13. Lu AJH, Hern TZ, Yang S, Siang KJ, Liu J. Advances in stem cell applications for wound healing. Adv Mod Biomed 2025;1:33-42.
14. Xu H, Liu J, Zhang Y, Zhou Y, Zhang L, Kang J, et al. KIF23, under regulation by androgen receptor, contributes to nasopharyngeal carcinoma deterioration by activating the Wnt/β-

catenin signaling pathway. Funct Integr Genomics 2023;23:116.
15. Bie G, Cheng S, Huang W, Yin Z, Liu J. CDCP1 promotes the malignant phenotypes of nasopharyngeal carcinoma via the Wnt/β-catenin signaling pathway. BMC Biotechnol 2025;25:67.
16. Shao YY, Wang HY, Hsu HW, Wo RR, Cheng AL, Hsu CH. Downregulation of PD-L1 expression by Wnt pathway inhibition to enhance PD-1 blockade efficacy in hepatocellular carcinoma. Biol Direct 2025;20:49.
17. Sun P, Qin W, Xu H, Yin H, Yang L, Zhang X, et al. SPTSSA facilitates gastric cancer progression with modulating PD-L1 in immunomicroenvironment through Wnt/β-catenin pathway. Cell Oncol (Dordr) 2025;48:1127-44.
18. Nkosi D, Crowe WE, Altman BJ, Oltvai ZN, Giampoli EJ, Velez MJ. SATB2 is an emergent biomarker of anaplastic thyroid carcinoma: a series with comprehensive biomarker and molecular studies. Endocr Pathol 2024;35:432-41.
19. Wang P, Zhu J, Long Q, Wang Y, Xu H, Tao H, et al. LncRNA SATB2-AS1 promotes tumor growth and metastasis and affects the tumor immune microenvironment in osteosarcoma by regulating SATB2. J Bone Oncol 2023;41:100491.
20. Lin C, Wu Y, Qian Y, Li J, He Y, Yu H, et al. SATB2 promotes radiation resistance of esophageal squamous cell carcinoma by regulating epithelial-to-mesenchymal transition via the Wnt/β-catenin pathway. Front Oncol 2025;15:1543426.
21. Ouyang X, Li S, Ding Y, Xin F, Liu M. Mechanism of miRNA-31 regulating Wnt/β-catenin signaling pathway by targeting Satb2 in the osteogenic differentiation of human bone marrow-derived mesenchymal stem cells. J Musculoskelet Neuronal Interact 2023;23:346-54.
22. Zeng Y, Duan T, Huang J, Wang X. Astragaloside IV inhibits nasopharyngeal carcinoma progression by suppressing the SATB2/Wnt signaling axis. Toxicol Res (Camb) 2025;14:tfaf047.
23. Liang Y, Chen B, Liang D, Quan X, Gu R, Meng Z, et al. Pharmacological effects of Astragaloside IV: a review. Molecules 2023;28:6118.
24. Chen M, Fu B, Zhou H, Wu Q. Therapeutic potential and mechanistic insights of astragaloside IV in the treatment of arrhythmia: a comprehensive review. Front Pharmacol 2025;16:1528208.
25. Cui Z, Shang Q. Mechanistic insights into the antitumor effects of astragaloside IV and astragalus polysaccharide in digestive system cancers. Front Pharmacol 2025;16:1691011.
26. Wu T, Wu S, Gao H, Liu H, Feng J, Yin G. Astragaloside IV augments anti-PD-1 therapy to suppress tumor growth in lung cancer by remodeling the tumor microenvironment. Eur J Histochem 2024;68:4098.
27. Ma Y, Li Y, Wu T, Li Y, Wang Q. Astragaloside IV attenuates programmed death-ligand 1-mediated immunosuppression during liver cancer development via the miR-135b-5p/CNDP1 axis. Cancers (Basel) 2023;15:5048.
28. Zhao J, Bang S, Furutani K, McGinnis A, Jiang C, Roberts A, et al. PD-L1/PD-1 checkpoint pathway regulates hippocampal neuronal excitability and learning and memory behavior. Neuron 2023;111:2709-26.e2709.
29. Onkar SS, Carleton NM, Lucas PC, Bruno TC, Lee AV, Vignali DAA, et al. The great immune escape: understanding the divergent immune response in breast cancer subtypes. Cancer Discov 2023;13:23-40.
30. Sadri FJ. PROTACs in colorectal cancer: a new era in targeted protein degradation therapy. Adv Clin Pharmacol Ther 2025;2:1-16.
31. Huang H, Li S, Tang Q, Zhu G. Metabolic Reprogramming and immune evasion in nasopharyngeal carcinoma. Front Immunol 2021;12:680955.
32. Li YC, Xiao YH, Chen FX, Xiao SY, Lin JM, Cai ST, et al. PXDN as a pan-cancer biomarker and promotes tumor progress via immune inhibition in nasopharyngeal carcinoma. Front Oncol 2024;14:1463011.
33. Dolton G, Rius C, Wall A, Szomolay B, Bianchi V, Galloway SAE, et al. Targeting of multiple tumor-associated antigens by individual T cell receptors during successful cancer immunotherapy. Cell 2023;186:3333-49.
34. Wu M, Huang Q, Xie Y, Wu X, Ma H, Zhang Y, et al. Improvement of the anticancer efficacy of PD-1/PD-L1 blockade via combination therapy and PD-L1 regulation. J Hematol Oncol 2022;15:24.
35. Wu CC, Chen MS, Lee TY, Huang TS, Cho DY, Chen JY. Epstein-Barr virus BRLF1 induces PD-L1 expression in nasopharyngeal carcinoma cells. Viral Immunol 2024;37:115-23.
36. Philip M, Schietinger A. CD8(+) T cell differentiation and dysfunction in cancer. Nat Rev Immunol 2022;22:209-23.
37. Xiang M, Yu Y, Gao Q, Xing J. MiR-425-5p mediation of malignant behavior and immune escape of cervical cancer cells by targeting NCAM1. Iran J Allergy Asthma Immunol 2025;24:834-50.
38. Duan J, Lin Y, He Z, Schachner M, Lin SL. Loss of B3GAT1/HNK-1 disrupts glioma-CD8(+) T cell immune synapse formation for immune escape. Int Immunopharmacol 2026;169:115877.
39. Su Z, Chen M, Ding R, Shui L, Zhao Q, Luo W. Long non−coding RNA HCG11 suppresses the malignant phenotype of non−small cell lung cancer cells by targeting a miR−875/SATB2 axis. Mol Med Rep 2021;24:552.
40. Roy SK, Shrivastava A, Srivastav S, Shankar S, Srivastava RK. SATB2 is a novel biomarker and therapeutic target for cancer. J Cell Mol Med 2020;24:11064-9.
41. Wang Y, Li CF, Sun LB, Li YC. microRNA-4270-5p inhibits cancer cell proliferation and metastasis in hepatocellular carcinoma by targeting SATB2. Hum Cell 2020;33:1155-64.
42. Wu X, Que H, Li Q, Wei X. Wnt/β-catenin mediated signaling pathways in cancer: recent advances, and applications in cancer therapy. Mol Cancer 2025;24:171.
43. Janeeh AS, Bajbouj K, Rah B, Abu-Gharbieh E, Hamad M. Interplay between tumor cells and immune cells of the colorectal cancer tumor microenvironment: Wnt/β-catenin pathway. Front Immunol 2025;16:1587950.
44. Liu W, Chen H, Wang D. Protective role of astragaloside IV in gastric cancer through regulation of microRNA-195-5p-mediated PD-L1. Immunopharmacol Immunotoxicol 2021;43:443-51.
45. Yang J, Wang J, Zhang W, He H, Wang C, Zhang Y, et al. Astragaloside IV directly targets PPP1R14B to sensitize prostate cancer to anti-PD-1 immunotherapy by remodeling the CX3CL1/CD8(+) T cell axis. Phytomedicine 2026;155:158158.
46. Kong C, Sun J, Hu X, Li G, Wu S. A tumor targeted nano micelle carrying astragaloside IV for combination treatment of bladder cancer. Sci Rep 2024;14:17704.
47. Tang J, Gao Y, Fu Y, Han Z, Xu P, Li X, et al. Astragaloside IV mitigates influenza-induced inflammatory responses by suppressing the Wnt/β-catenin signalling pathway in alveolar macrophages. Vet Res 2025;56:95.
48. Wu Y, Yin M, Xia W, Dou B, Liu X, Sun R. Enhancing NK cell antitumor activity with natural compounds: research advances

and molecular mechanisms. Phytother Res 2025;39:1905-29.
49. Lin Z, Cao R, Guo X, Nie F, Xu J, Guo Y. Herbal Medicine-derived natural product self-assembled nanoparticles: orchestrating chemo-chemodynamic-immunotherapy for tumor combination therapy. Adv Healthc Mater 2025;14:e2500913.
50. Deng LJ, Qi M, Li N, Lei YH, Zhang DM, Chen JX. Natural products and their derivatives: Promising modulators of tumor immunotherapy. J Leukoc Biol 2020;108:493-508.

Received: 4 February 2026. Accepted: 8 May 2026.

Licensee PAGEPress, Italy
European Journal of Histochemistry 2026; 70:4544
doi:10.4081/ejh.2026.4544